Resistivity size effect in epitaxial Rh(001) and Rh(111) layers

Atharv Jog, Tianji Zhou, and Daniel Gall

Abstract—Rh(001) and Rh(111) layers with thickness d =8-181 nm are sputter deposited onto MgO(001) and Al₂O₃(1120) substrates and their resistivity ρ measured in situ and ex situ at room-temperature and 77 K in order to quantify the resistivity size effect. Rh(001) layers are epitaxial single crystals and show a resistivity increase with decreasing d that is well described with the classical Fuchs and Sondheimer model, indicating an effective electron mean free path $\lambda_{eff} = 9.5 \pm 0.8$ nm at 295 K. Rh(111) layers exhibit an epitaxial microstructure with two 60°-rotated domains with a lateral width of 19±2 nm, as determined from the x-ray coherence length. The grain boundaries between the domains cause a thickness-independent resistivity contribution $\Delta \rho_{\rm gb} = 0.74$ and 0.59 $\mu\Omega$ cm at 295 and 77 K, indicating an electron reflection coefficient $R = 0.16 \pm 0.03$ for a boundary characterized by a 60° rotation about the <111> axis. Air exposure causes a nearly negligible (< 6%) resistivity increase which suggests a possible reduction in the surface scattering specularity by $\Delta p_1 = -0.3 \pm 0.2$ during surface oxidation. The overall results yield a temperatureindependent product of the bulk resistivity times the electron mean free path $\rho_0 \lambda = (4.5 \pm 0.4) \times 10^{-16} \,\Omega \text{m}^2$. This is 1.4 times larger than previously predicted from first principles, but 33%, 55%, 63%, and 11% smaller than for Cu, W, Co, and Ru, respectively, suggesting great promise for Rh as an alternative metal for narrow interconnects.

Index Terms—Interconnects, Rhodium, BEOL, MOL, Resistivity Scaling, Mean Free Path, Surface Scattering, Grain Boundary Scattering, Alternative Metals, Reflection Coefficient

I. INTRODUCTION

The continued downscaling of integrated circuits has led to major challenges in the Cu interconnect technology in terms of performance [1]–[4] and reliability [5]–[7]. As the interconnect line widths approach the electron-phonon scattering mean free path λ , the resistivity increases significantly due to electron scattering at surfaces [8]–[10] and grain boundaries [11], [12]. This resistivity size effect is often described using semi-classical transport models which employ the Boltzmann transport equation, assume an isotropic electron-phonon scattering cross-section, and treat surface and grain boundary scattering as boundary conditions [8], [9], [11]. These models predict an additive resistivity contribution that is proportional to $\rho_0 \lambda/d$, where ρ_0 is the bulk resistivity and d is the wire width or the grain size for surface and grain boundary scattering, respectively [8]–[11]. Hence, in the limit

This work was supported in part by SRC under tasks 2966 and 2881, the NY State Empire State Development's Division of Science, Technology and Innovation (NYSTAR) through Focus Center-NY-RPI Contract C150117, and the NSF under grant No. 1712752. The authors thank Katharine Dovidenko for help with EBSD.

of narrow conducting wires with a given geometry, the material with the smallest $\rho_o \lambda$ is expected to be most conductive [13], [14]. This argument neglects variations in the structure and chemistry of surfaces and grain boundaries which, in turn, affect the surface scattering specularity [4], [15]–[19] and the grain boundary reflection coefficient [20]–[26], respectively. Nevertheless, the product $\rho_o \times \lambda$ is a useful starting point to search for metals that can form narrow interconnect lines with a relatively low resistivity.

Rhodium has a predicted $\rho_0 \lambda = 3.23 \times 10^{-16} \ \Omega \text{m}^2$ which is smaller than that of any other elemental metal, suggesting a particularly small resistivity scaling [14], [27]. The corresponding predicted room-temperature mean free path λ = 6.88 nm is 5.8 times smaller than for Cu. In addition, Rh has a 1.64 times higher cohesive energy than Cu [28], indicating a higher temperature stability, a higher resistance to electromigration, and the potential for barrierless metallization [29], [30]. This makes Rh is a particularly promising potential replacement metal for narrow high-conductivity interconnect lines. However, we note that the first-principles prediction of a low $\rho_0 \lambda$ product is no guarantee for a small resistivity scaling [31], since such predictions are based on classical transport models which deviate from the quantum mechanical description [32]–[35], diverge from experimental measurements for narrow (< 10 nm) conductors [36]-[39], and are also affected by surface and grain boundary scattering parameters [15]–[24]. Therefore, an experimental verification of the low resistivity scaling of Rh is required.

In this paper, we experimentally quantify the resistivity size effect in Rh layers. For this purpose, Rh(001) and Rh(111) layers with thickness ranging from d=8 to 181 nm are sputter deposited on MgO(001) and Al₂O₃(11 $\bar{2}$ 0) substrates at $T_s=350$ °C and annealed *in situ* at 450, 550, 650, and 750 °C for 30 min each to reduce the surface roughness. The epitaxial growth on MgO(001) yields Rh(001) layers without grain boundaries, such that electron surface scattering can be quantified without confounding effects from scattering at grain boundaries. In contrast, the Rh(111) layers have two epitaxial domains and electron scattering at domain walls causes an additional resistivity contribution. Quantification of this effect suggests a 16% probability for electron reflection at the domain walls, which are grain boundaries characterized by a 60° rotation about the <111> axis. The overall results indicate a lower-

The authors are with the Department of Materials Science and Engineering, Rensselaer Polytechnic Institute, 110 8th St, Troy, NY 12180, USA.

bound room-temperature effective mean free path for Rh of 9.5 nm, and a temperature-independent $\rho_o\lambda$ product of (4.5 ± 0.4) ×10⁻¹⁶ Ω m². This is 1.4 times larger than predicted, but still smaller than competing interconnect metals including Cu, W, Co, Ru, suggesting the potential for Rh as metal for narrow interconnects.

II. PROCEDURE

Rhodium thin films were deposited on polished MgO(001) and Al₂O₃(1120) substrates in a three chamber ultra-high vacuum magnetron sputter deposition system with a 10⁻⁹ Torr base pressure [40]. Substrates were cleaned by successive ultrasonic baths in trichloroethylene, acetone, iso-propyl alcohol and deionized water for 15 min each. They are then blown dry with nitrogen and mounted onto a Mo holder using colloidal silver paint, introduced into the sputter deposition system via a load lock, and degassed in vacuum at 1000 °C for 1 hour. Deposition was performed at $T_s = 350$ °C in 4.5 mTorr 99.999% pure Ar using a constant power of 40 W applied to a 99.9% pure Rh target facing a continuously rotating substrate at a distance of 9 cm with a 45° tilt, yielding a deposition rate of 0.16 ± 0.01 nm/s. The deposition time was adjusted to obtain a series of Rh layers with thickness d = 8-181 nm, as measured by x-ray reflectivity for layers with $d \le 33.6$ nm and determined from the deposition rate for $d \ge 90.6$ nm.

Immediately after deposition, the substrate temperature was raised to 450, 550, 650, and 750 °C for 30 min each. This postdeposition vacuum annealing process is similar to what has previously been used for epitaxial Co(0001) and Ru(0001) layers [39], [41]–[43] and was done in order to improve the crystalline quality and reduce the surface roughness while the initially relatively low deposition temperature minimizes nuclei size and therefore facilitates continuous layers even at small thickness. After annealing, the samples were allowed to cool to room temperature in vacuum for 12 hours, followed by transport in vacuum to an analysis chamber for in situ resistivity measurements using a current of 1-100 mA applied to the outer probes of a linear four-point probe with spring loaded tips and a 1.0 mm inter-probe spacing. Samples were removed from the deposition chamber via a load lock vented to atmospheric pressure using dry N₂ and were immersed in liquid N₂ within 2 s to limit air exposure and possible Rh surface oxidation. Resistivity measurements at 77 K were taken with a similar linear four-point probe with both sample and probe tips completely immersed in liquid N₂. Subsequent ex situ measurements were performed with the same setup after the samples were warmed to room temperature by blowing dry N₂ to minimize ice/water built-up on the Rh surface.

X-ray diffraction (XRD) and X-ray reflectivity (XRR) analyses were performed using a PANalytical X'pert PRO MPD system with a Cu source and a parabolic mirror yielding a parallel beam with a <0.055° divergence and a 0.27° parallel plate collimator in front of a PIXcel solid-state line detector operating in receiving mode with a 0.165 mm active length, corresponding to a 2θ opening of < 0.04°. Rocking curves were acquired by scanning in ω while keeping the 2θ value fixed to detect the desired 002 or 111 reflections. ϕ -scans were acquired using a poly-capillary lens providing a point source with quasiparallel Cu K α X-rays with a divergence of less than 0.3°, a

fixed 2θ value corresponding to Rh 113 reflections, and an offset in ω of 25.24° and 29.50° for 001 and 111 oriented layers, respectively.

Crystallographic orientation maps and pole figures were obtained using electron backscatter diffraction (EBSD) in a VERSA SEM column with a NordlysNano detector from Oxford Instruments at a pressure of 10⁻³ torr. Secondary electron micrographs and backscatter patterns were obtained with a 10 keV and 1 nA electron beam at a 13 mm working distance. The collected patterns were acquired and analyzed using the Flamenco acquisition software and the HKL Channel 5 software packages from Oxford Instruments, respectively.

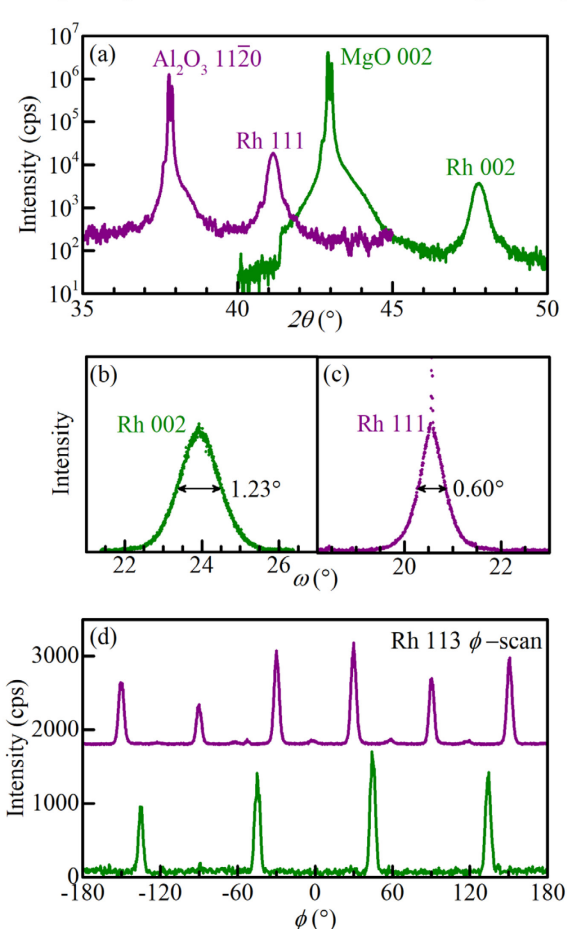


Figure 1. Representative (a) θ - 2θ scan, (b) ω -rocking curve of Rh 002 reflection, (c) ω -rocking curve of Rh 111 reflection, and (d) Rh 113 ϕ -scan from a Rh(001)/MgO(001) layer with thickness d=33.4 nm (green) and a Rh(111)/Al₂O₃(11 $\overline{2}$ 0) layer with d=33.6 nm (purple).

III. RESULTS

Figure 1 shows typical x-ray diffraction results which demonstrate that the series of Rh layers deposited on MgO(001) substrates are epitaxial Rh(001) while deposition on Al₂O₃(11 $\overline{2}$ 0) substrates yields 111-oriented layers with a two-domain microstructure. More specifically, the θ -2 θ scan from a 33.4 nm-thick Rh/MgO(001) layer plotted in green in Fig. 1(a) shows a strong double-peak feature at 2θ = 42.92 and 43.03° which is attributed to the MgO 002 Cu K_{a1} and K_{a2} reflections and a peak at 2θ = 47.78° which is attributed to Rh 002. This is the only detected peak from the Rh layer over the entire

measured $2\theta = 10-90^{\circ}$ range, indicating a 001-orientation of this layer. The intensity discontinuity at $2\theta = 41.33^{\circ}$ is an experimental artifact due to the strong intensity from the substrate reflection and related to electronic noise in the solidstate line-detector. Fig. 1(b) shows the ω -rocking curve of the Rh 002 peak from the same sample. It has a full-width at halfmaximum (FWHM) of 1.23°, confirming the strong 001 orientation of this layer. A ϕ -scan from the asymmetric Rh 113 reflection from the same sample is shown in Fig. 1(d). It is obtained with a constant ω -offset of 25.24° and shows four peaks at -135°, -45°, 45°, and 135°, indicating four-fold inplane rotational symmetry and demonstrating that growth on MgO(001) leads to epitaxial single-crystal Rh(001) layers with a cube-on-cube orientation relationship with the substrate: $Rh(001) \parallel MgO(001)$ and $Rh[100] \parallel MgO[100]$. The same epitaxial relationship has previously been reported for sputter deposited Rh on MgO [44].

Fig. 1 also shows corresponding XRD results from a 33.6nm-thick Rh layer deposited on $Al_2O_3(11\bar{2}0)$, plotted as purple lines in Figs. 1(a,c,d). The θ -2 θ pattern in Fig. 1(a) shows the substrate peaks at $2\theta = 37.78$ and 37.88° and the only detectable peak from the Rh layer at $2\theta = 41.14^{\circ}$, indicating a 111 out-ofplane orientation. The ω -rocking curve from the 111 reflection of this layer in Fig. 1(c) has a FWHM of 0.60°. This width is determined by excluding the very sharp peak with a 0.026° width that appears on top of the broader curve and suggests that a small portion of the Rh(111) layer forms fully-strained, wellaligned, low-defect-density crystallites. The corresponding Rh 113 ϕ -scan in Fig. 1(d) is collected using an ω -offset of 29.50°. It exhibits six peaks which are separated by 60°, indicating two 111-oriented Rh domains that are 60° rotated with respect to each other, where Rh(111) \parallel Al₂O₃ (11 $\bar{2}$ 0) and either Rh[$\bar{2}$ 11] or Rh[$\overline{1}2\overline{1}$] || Al₂O₃[0001]. Six additional peaks which have a 2-orders-of-magnitude lower intensity and are shifted by 30° in ϕ with respect to the primary peaks can be detected and indicate a minor secondary set of in-plane orientations that are neglected in the following, as they represent only approximately 1% of the layer volume. The two primary epitaxial 60° rotated domains are separated by grain boundaries which cause electron scattering, as discussed in Section IV. The average distance between grain boundaries is equal to the average domain width D and is estimated by setting it equal to the in-plane coherence length [40]. More specifically, the 0.60° FWHM of the rocking curve for this 33.6-nm-thick Rh(111) layer yields an estimated D = 21 nm. Similar XRD analyses on other samples indicate that the domain width is nearly independent of the layer thickness, with D = 19, 17, and 21 nm for d = 8.6, 16.7, and 33.6 nm, respectively. Thus, overall, the Rh(111) layers have a thickness-independent $D = 19\pm 2$ nm. For comparison, the Rh(001) layer rocking-curve FWHM peak widths are 1.73°, 1.64°, 1.23°, and 0.80° for d = 8.3, 16.6, 33.4, and 90.6 nm, respectively. These layers are single crystals (i.e. a single grain orientation) except the 16.6-nm-thick Rh(001) layer which exhibits a multi-domain polycrystalline microstructure with both 001 and 111 oriented epitaxial domains with one and four distinct in-plane orientations, respectively. This layer has a very narrow 0.054° rocking curve width from the 111-domains, indicating a 236 nm lateral

coherence length and a correspondingly negligible $0.05~\mu\Omega$ cm resistivity contribution from electron scattering at grain boundaries, which is an order of magnitude smaller than for the Rh(111) layers, as discussed in Section IV.

Figure 2 shows secondary electron SEM micrographs, EBSD inverse pole figure (IPF-X) orientation maps and {111} pole figures for Rh layers grown on MgO(001) and Al₂O₃ (11 $\bar{2}$ 0) substrates. The micrograph in Fig. 2(a) from a Rh(001)/MgO(001) layer with d = 33.4 nm exhibits a few minor voids (<1 % of surface) but otherwise negligible contrast variations. The corresponding IPF-X orientation map in Fig. 2(b) from the same area of the surface is completely red, indicating a single Rh in-plane orientation. More specifically, as indicated by the unit orientation triangle for the cubic crystal system in the inset, Rh [100] is aligned with the horizontal xaxis which also corresponds to the MgO [100] direction. This confirms the single-crystal Rh(001)/MgO(001) cube-on-cube epitaxial relationship, as also determined by XRD analyses and indicated by the arrows in Fig. 2(a). This is also consistent with the Rh{111} pole figure in Fig. 2(c) showing a single-set of four-fold symmetric peaks at a 54° tilt.

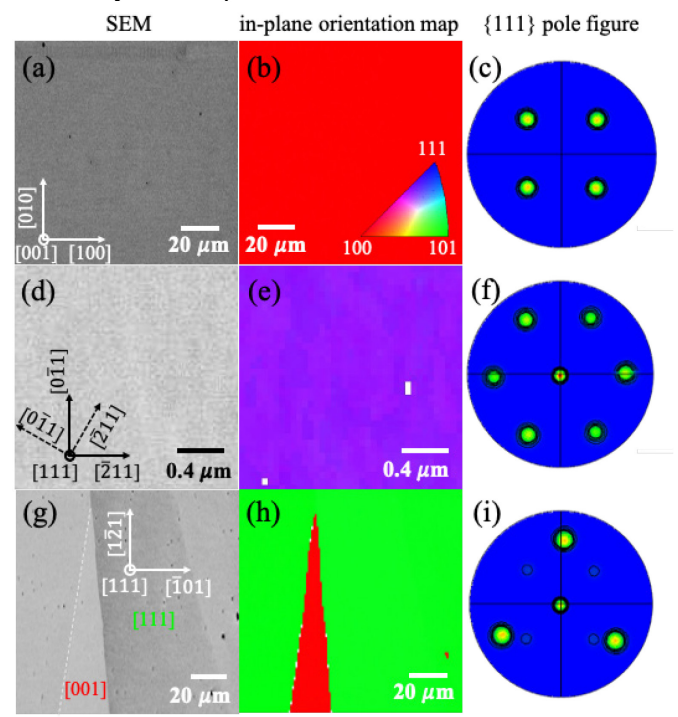


Figure 2. Scanning electron micrographs (SEM), in-plane orientation maps, and corresponding Rh $\{111\}$ EBSD pole figures for Rh layers on MgO(001) with d = 33.4 nm (a,b,c), on Al₂O₃(**11** $\overline{\bf 20}$) with d = 33.6 nm (d,e,f), and on MgO(001) with d = 16.6 nm (g,h,i).

Corresponding data from a 33.6-nm-thick Rh(111) layer grown on Al₂O₃(11 $\overline{2}$ 0) is shown in Figs. 2(d,e,f). The central peak in the {111} pole figure in Fig. 2(f) confirms the 111 growth direction and the set of six poles at a 70° tilt indicate the presence of two three-fold symmetric domains which are rotated by 60° from each other, as indicated with the solid and dashed arrows in Fig. 2(d). The IPF-X orientation map in Fig. 2(e) cannot resolve the two domains despite the higher magnification (see scale bar), but shows slight color variations from purple to violet which indicate a Rh< $\overline{2}$ 11> type in-plane orientation along the horizontal direction of the micrograph

which corresponds to the in-plane Al₂O₃[0001] direction of the substrate. Thus, this analysis confirms the two epitaxial domains with $Rh[\bar{2}11] || Al_2O_3[0001]$ or $Rh[\bar{1}2\bar{1}] || Al_2O_3[0001]$, while the domain size is below the detection limit / resolution of our EBSD analysis. The bottom row in Fig. 2 shows data from the unique Rh layer deposited on MgO(001) with d = 16.6nm, which exhibits both 111 and 001 oriented domains as determined by XRD. The micrograph in Fig. 2(g) shows a slightly higher void density than in Fig. 2(a), as expected for a layer with half the thickness. The IPF-X orientation map in Fig. 2(h) shows just two grains despite the relatively low magnification, indicating grain sizes $> 50 \mu m$. This is a quite unique microstructure, considering the small layer thickness of only 16.6 nm and suggests (i) epitaxial growth for Rh(001)/MgO(001) for the red grain and (ii) a fast lateral growth after nucleation of a 111-oriented grain with Rh[101] || MgO[100] (green). The orientation of the green domain is indicated by the arrows in Fig. 2(g), but arrows for the Rh(001) grain are omitted due to the limited size of the grain, which is simply labeled with a red "[001]" instead. The corresponding pole figure in Fig. 2(i) has a single set of 3-fold symmetric 111poles at a 70° tilt and four weak poles at a 54° tilt, indicating a 111 and 001 oriented grain, respectively, each with a single inplane orientation. This data is consistent with the XRD results and indicates that this Rh layer exhibits a multi-domain polycrystalline microstructure with both 001 and 111 domains, but with very large domain sizes such that electron-scattering at the boundaries is negligible.

Roughness measurements by XRR indicate root-mean-square surface and interface roughness values <0.3 nm for all Rh(001) and Rh(111) layers, as listed in Table 1. These small values indicate smooth interfaces which are expected to have a negligible effect on electron surface scattering [45].

| Thickness (nm) | Roughness (nm) | | Resistivity (μΩcm) | | |
|----------------|--|--------------|--------------------|-----------------|-----------------|
| | | | 295 K | | 77 K |
| | $\sigma_{\!\scriptscriptstyle \mathrm{S}}$ | σ_{i} | In situ | Ex situ | Ex situ |
| | | | Rh(001) | | |
| 8.3 ± 0.2 | 0.14 | 0.30 | 7.67 ± 0.18 | 7.98 ± 0.19 | 2.92 ± 0.07 |
| 16.6 ± 0.1 | 0.10 | 0.21 | 5.69 ± 0.05 | 6.03 ± 0.05 | 1.51 ± 0.01 |
| 33.4 ± 0.2 | 0.15 | 0.30 | 5.37 ± 0.03 | 5.38 ± 0.04 | 1.23 ± 0.01 |
| 90.6 ± 2.6 | 0.12 | 0.37 | 4.82 ± 0.14 | 4.95 ± 0.15 | 0.82 ± 0.02 |
| 181 ± 3 | - | - | 4.67 ± 0.26 | 4.81 ± 0.27 | 0.67 ± 0.05 |
| | | | Rh(111) | | |
| 8.6 ± 0.2 | 0.10 | 0.30 | 8.05 ± 0.18 | 8.34 ± 0.19 | 3.06 ± 0.07 |
| 16.7 ± 0.1 | 0.17 | 0.12 | 6.60 ± 0.07 | 6.75 ± 0.04 | 2.27 ± 0.03 |
| 33.6 ± 0.4 | 0.23 | 0.25 | 5.99 ± 0.08 | 6.03 ± 0.08 | 1.69 ± 0.02 |
| 90.8 ± 0.6 | - | - | 5.44 ± 0.03 | 5.48 ± 0.03 | 1.21 ± 0.01 |

Table 1. Thickness, root-mean-square surface σ_s and interface σ_t roughness, and resistivity of epitaxial Rh(001) and Rh(111) layers measured *in situ* and *ex situ* at 295 K and *ex situ* immersed in liquid nitrogen at 77 K.

Figure 3 shows the resistivity ρ vs thickness d of epitaxial Rh(001) deposited on MgO(001) and two-domain Rh(111) layers deposited on Al₂O₃(11 $\bar{2}$ 0) substrates, as measured *in situ* at 295 K and *ex situ* immersed in liquid nitrogen at 77 K. The plotted data is also summarized in Table 1. Green squares in Fig. 3 indicate the room temperature resistivity of Rh(001). It is $4.67 \pm 0.26 \,\mu\Omega$ cm for the largest thickness $d=181 \pm 3$ nm which is identical to the reported Rh bulk resistivity $\rho = 4.7 \,\mu\Omega$ cm [46], indicating negligible electron scattering at surfaces for the layer with $d=181 \pm 3$ nm at 295 K. The resistivity increases

with decreasing Rh(001) film thickness d = 90.6, 33.4, 16.6, and 8.3 nm to $\rho = 4.82 \pm 0.14$, 5.37 ± 0.03 , 5.69 ± 0.05 , and 7.67 \pm $0.18 \mu\Omega$ cm, respectively. This is due to electron surface scattering, as discussed in more detail in Section IV. The room temperature resistivity measured ex situ after air exposure (see Table 1) is slightly larger but within 6% of the *in situ* measured ρ , suggesting that oxygen exposure has only a minor effect on the resistivity of these layers. The Rh(001) resistivity at 77 K, plotted in Fig. 3 as green diamonds, is $\rho = 0.67 \pm 0.05 \,\mu\Omega$ cm for d = 181 nm. This is 45% larger than the reported 77 K bulk resistivity of 0.46 $\mu\Omega$ cm [46]. The deviation is partially attributed to electron surface scattering which becomes more important at lower temperatures due to the larger electronphonon scattering mean free path, resulting in a surface scattering resistivity contribution for this layer of 0.10 $\mu\Omega$ cm, based on the quantitative analysis discussed in Section IV. Similar to the room temperature data, the ρ at 77 K increases with decreasing d. However, the absolute values are smaller than at 295 K, due to the smaller electron-phonon scattering. The resistivity difference $\Delta \rho$ between the two temperatures is nearly independent of thickness, with $\Delta \rho = 4.00, 4.00, 4.14$, 4.18, and 4.75 $\mu\Omega$ cm for the five samples with decreasing d =181-8.3 nm. This indicates that the resistivity contributions from electron scattering at surfaces and phonons are approximately additive, following Matthiessen's rule. We note that the reduced phonon-scattering at 77 K makes the relative importance of surface scattering much more pronounced at 77 K. More specifically, the room-temperature resistivity increases by 64% as d is reduced from 181 to 8.3 nm, while the corresponding increase is 335% at 77 K.

The plot in Fig. 3 also shows the resistivity vs thickness data from four two-domain epitaxial Rh(111) layers deposited on $Al_2O_3(11\bar{2}0)$. The room-temperature resistivity indicated by the purple triangles increases with decreasing d = 90.8, 33.6,16.7, and 8.6 nm from $\rho = 5.44 \pm 0.03$ to 5.99 ± 0.08 , $6.60 \pm$ 0.07, and $8.05 \pm 0.18 \,\mu\Omega$ cm. These values are larger than for the Rh(001) samples, indicating additional electron scattering at grain boundaries, as discussed in Section IV. We note that the resistivity is nearly unaffected (< 4% increase) by air exposure, similar to the result from the Rh(001) layers. The 77 K resistivity of Rh(111) layers plotted as purple hexagons is ρ = $1.21 \pm 0.01 \,\mu\Omega$ cm for d = 90.8 nm. This is 163% larger than the reported Rh bulk resistivity at 77 K, indicating the increased relative importance of both surface and defect scattering at low temperature. The absolute resistivity increase with decreasing d is similar at 77 and 295 K, with a resistivity difference between the two temperatures of $\Delta \rho = 4.99, 4.33, 4.30, \text{ and } 4.23 \ \mu\Omega\text{cm}$ with increasing d = 8.6-90.8 nm.

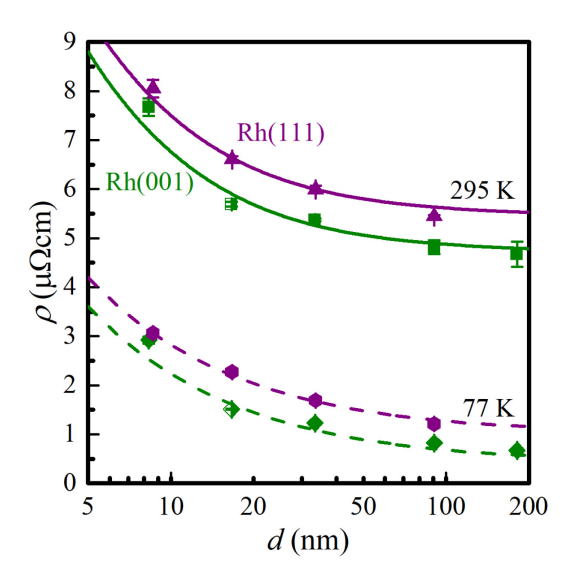


Figure 3. Resistivity ρ vs thickness d, measured in situ (green squares, purple triangles) at 295 K and immersed in liquid nitrogen at 77 K (green diamond and purple hexagons), from epitaxial Rh(001)/MgO(001) and two-domain Rh(111)/Al₂O₃(11 $\overline{2}$ 0) layers, respectively.

IV. DISCUSSION

We now discuss the electron transport in our Rh(001) and Rh(111) layers using the classical transport models by Fuchs and Sondheimer (FS) for surface scattering [8], [9] and by Mayadas and Shatzkes (MS) for grain boundary scattering [11]. We start our analysis by applying the FS model to the data from the Rh(001) layers, because these epitaxial single-crystal layers have no grain boundaries such that contributions from the MS model can be neglected. The FS model quantifies the resistivity contribution from surface scattering using two parameters: the surface scattering specularity p and the electron phonon scattering mean free path λ , where the former can be further divided into p_1 for scattering at the Rh top surface and p_2 for scattering at the Rh-substrate interface [12], [15]. The two parameters p and λ are strongly correlated such that data fitting usually does not allow to uniquely determine both [47], [48]. To circumvent this problem, we set $p_1 = p_2 = 0$ (assuming electron surface scattering is completely diffuse) and obtain a lower bound to the effective mean free path λ_{eff} by fitting a FS curve to the measured resistivity using the exact version of the FS model [41], [47], [48]. The solid and dashed green lines in Fig. 3 are the results from such curve fitting. For this purpose, the Rh bulk resistivity is fixed to the reported values of $\rho_0 = 4.7$ and 0.46 μΩcm at 295 and 77 K, respectively [49]. With this approach, the electron mean free path is the only fitting parameter and is determined to be $\lambda = 9.5 \pm 0.8$ nm at 295 K and $\lambda = 102 \pm 8$ nm at 77 K. That is, λ at 77 K is an order of magnitude larger than at room temperature, which is due to the reduced electron-phonon scattering at low temperatures which also results in an order-of-magnitude smaller bulk resistivity. We determine values for the product $\rho_0 \lambda$ of $(4.5 \pm 0.4) \times 10^{-16}$ and $(4.7 \pm 0.4) \times 10^{-16} \Omega \text{m}^2$ from the 295 and 77 K data, indicating that $\rho_0\lambda$ is temperature-independent within the experimental uncertainty, as expected from classical transport models. However, our measured in situ $\rho_0\lambda$ value is 39% larger than the reported first-principles prediction for Rh. Such deviations have

been reported for various metals including Ni [47], Nb [48], Co [39], and W [50], and have been attributed to (a) the failure of the classical FS model to describe resistivity scaling at small thicknesses which assumes a bulk-like electronic structure [32] or (b) contributions to resistivity due to strain fields from misfitdislocations which become increasingly important as the thickness is reduced [31]. Nevertheless, the small value of the measured electron mean free path $\lambda = 9.5 \pm 0.8$ nm at 295 K and the corresponding $\rho_0 \lambda = (4.5 \pm 0.4) \times 10^{-16} \,\Omega \text{m}^2$ suggest a small resistivity scaling for Rh. More specifically, the measured $\rho_0\lambda$ for Rh is 1.5, 2.2, 2.7, and 1.1 times smaller than the reported values for competing interconnect materials like Cu with $6.7 \times 10^{-16} \Omega \text{m}^2$ [15], W with $10.1 \times 10^{-16} \Omega \text{m}^2$ [50], Co with $12.2 \times 10^{-16} \Omega m^2$ [39], and Ru with $5.06 \times 10^{-16} \Omega m^2$ [41], respectively, indicating great promise for Rh as an alternative metal for narrow high-conductivity interconnects.

We discuss, as a second step, the resistivity of the Rh(111) layers that are grown on $Al_2O_3(11\bar{2}0)$ substrates and form epitaxial layers with a two-domain microstructure, as indicated by our XRD analyses. Rh(111) layers have a higher overall resistivity compared to the Rh(001) layers of similar thicknesses. This is attributed to additional electron scattering at the domain walls which are vertical grain boundaries. The approximate form of the MS model [12] predicts that electron scattering at grain boundaries causes an additive resistivity term $\Delta \rho_{\rm gb} = 3 \rho_{\rm o} \lambda R / [2D(1-R)]$ which is a function of the $\rho_{\rm o} \lambda$ product, the grain size D and the reflection coefficient R. Our XRD results indicate that the grain boundary type (60° rotation about the 111-axis) as well as the domain width $D = 19\pm 2$ nm are independent of the Rh(111) layer thickness. Thus, R and D and, in turn $\Delta \rho_{\rm gb}$, are expected to be independent of d for the Rh(111) sample series. Correspondingly, data fitting of the Rh(111) resistivity in Fig. 3 is done by adding a constant $\Delta \rho_{\rm gb}$ to the FS prediction. This yields the purple solid and dashed lines which are shifted with respect to the green lines by a constant $\Delta \rho_{\rm gb} =$ 0.74 and 0.59 u Ω cm for 295 and 77 K, respectively. These lines describe the measured ρ of Rh(111) samples well, confirming the additive resistivity contribution from electron scattering at domain walls. We determine the reflection coefficient R with the approximate MS expression, using the $\Delta \rho_{\rm gb}$ from data fitting, the measured $\rho_o \lambda$ from the Rh(001) data at 295 and 77 K, and by setting the grain size equal to the lateral x-ray coherence length $D = 19\pm 2$ nm. This yields $R = 0.17 \pm 0.02$ and 0.14 ± 0.02 at 295 and 77 K, respectively, or a combined R = 0.16 ± 0.03 . The latter average is taken because, within the approximate classical models, grain boundary scattering is temperature independent. The $R = 0.16 \pm 0.03$ can be directly compared to reported first-principles predictions R = 0.13, 0.56, 0.50, and 0.36 for the Rh coincidence-lattice grain boundaries $\Sigma 3$, $\Sigma 5$, $\Sigma 9$, and $\Sigma 11$, respectively [27]. Our measured R is close to the predicted R = 0.13 for $\Sigma 3$, which is the <111> twin boundary. Interestingly, our domain boundary and the $\Sigma 3$ twin boundary are very similar: they both are a boundary between two grains which are related to each other by a 60° rotation about a <111> axis. However, they are distinct because the normal of the boundary plane is perpendicular to the <111> rotation axis for the domain walls, but is parallel for the $\Sigma 3$ boundary. The fact that R of these two boundaries is approximately the same suggests that the reflection coefficient

is primarily determined by the relative orientation of the Fermi surface in the two grains, while the atomic structure of the actual boundary which determines the potential variation across the boundary is of secondary importance or even negligible [31]. We note that $R = 0.16 \pm 0.03$ is for a high-symmetry boundary, while the reflection probability at a random grain boundary is expected to be considerably higher. This has previously been demonstrated for Cu, which has an experimentally measured range of R = 0.2-0.8, with an average R = 0.3 for random boundaries [12], [20], [51], [52], while the symmetric $\Sigma 3$, $\Sigma 5$, $\Sigma 9$, and $\Sigma 11$ boundaries have more than two times smaller reflection coefficients, with first-principles predictions of R = 0.016 - 0.02, 0.13 - 0.145, 0.14 - 0.164, and 0.07-0.0772 for these four boundaries, respectively [21], [26]. Thus, assuming that random boundaries have a larger R than the calculated symmetric boundaries (as for Cu), we expect R > 0.6for random Rh grain boundaries.

The slight increase in the measured resistivity upon air exposure of both the Rh(001) and Rh(111) sample series can be attributed to experimental uncertainty but may also indicate an increase in diffuse surface scattering during surface oxidation, similar to what has been reported for Ni [47], Nb [48], and Cu [15]. We follow the procedures in [47], [48] to quantitatively analyze our *ex situ* room temperature resistivity data. This suggests that air-exposure causes a decrease in the room-temperature scattering specularity $\Delta p_1 = -0.24 \pm 0.14$ for the Rh(001) top surface and a corresponding $\Delta p_1 = -0.33 \pm 0.25$ for the Rh(111) surface, or a combined average $\Delta p_1 = -0.3 \pm 0.2$. This decrease in p_1 is smaller than the $\Delta p_1 = -0.6$ or -0.7 that has been reported for Cu [4], [15], indicating that the resistivity size effect in Rh is less affected by surface oxidation than for

REFERENCES

- [1] S. Dutta, K. Moors, M. Vandemaele, and C. Adelmann, "Finite Size Effects in Highly Scaled Ruthenium Interconnects," *IEEE Electron Device Lett.*, vol. 39, no. 2, pp. 268–271, Feb. 2018, doi: 10.1109/LED.2017.2788889.
- [2] Wei Wang, T. Spooner, Chih-Chao Yang, and XunYuan Zhang, "Geometry impact on the reduction of Cu interconnect wire resistance," in 2016 IEEE International Interconnect Technology Conference / Advanced Metallization Conference (IITC/AMC), May 2016, pp. 144– 146, doi: 10.1109/IITC-AMC.2016.7507712.
- [3] C. Witt, F. Baumann, E. Huang, and D. Rath, "Resistance contributions to copper interconnects," in 2017 IEEE International Interconnect Technology Conference (IITC), May 2017, pp. 1–3, doi: 10.1109/IITC-AMC.2017.7968975.
- [4] E. Milosevic and D. Gall, "Copper Interconnects: Surface State Engineering to Facilitate Specular Electron Scattering," *IEEE Trans. Electron Devices*, vol. 66, no. 6, pp. 2692–2698, Jun. 2019, doi: 10.1109/TED.2019.2910500.
- [5] J. S. Chawla, S. H. Sung, S. A. Bojarski, C. T. Carver, M. Chandhok, R. V. Chebiam, J. S. Clarke, M. Harmes, C. J. Jezewski, M. J. Kobrinski, B. J. Krist, M. Mayeh, R. Turkot, and H. J. Yoo, "Resistance and electromigration performance of 6 nm wires," in 2016 IEEE International Interconnect Technology Conference / Advanced Metallization Conference (IITC/AMC), May 2016, pp. 63–65, doi: 10.1109/IITC-AMC.2016.7507682.
- [6] C. L. Lo, K. Zhang, J. A. Robinson, and Z. Chen, "BEOL compatible subnm diffusion barrier for advanced Cu interconnects," 2018 Int. Symp. VLSI Technol. Syst. Appl. VLSI-TSA 2018, pp. 1–2, 2018, doi: 10.1109/VLSI-TSA.2018.8403818.
- [7] O. V. Pedreira, K. Croes, A. Lesniewska, C. Wu, M. H. van der Veen, J. de Messemaeker, K. Vandersmissen, N. Jourdan, L.G. Wen, C. Adelmann, B. Briggs, V. V. Gonzalez, J. Bömmels, Zs. Tökei.,

Cu.

V. CONCLUSIONS

In situ and low-temperature transport measurements on single-crystal Rh(001) layers deposited on MgO(001) substrates show a resistivity increase that is well described with the FS model and diffuse surface scattering, yielding an effective room-temperature mean free path $\lambda_{eff} = 9.5 \pm 0.8$ nm and a temperature-independent product $\rho_0 \lambda = (4.5 \pm 0.4) \times 10^{-16}$ Ω m². Rh(111) layers deposited on Al₂O₃(11 $\bar{2}$ 0) exhibit a microstructure with two 60°-rotated domains. Their resistivity is higher than for the Rh(001) layers, which is attributed to electron scattering at the domain walls, with an electron reflection probability $R = 0.16 \pm 0.03$. This value is for grain boundaries characterized by a 60° rotation about the <111> axis and matches the previously predicted R for $\Sigma 3$ twin boundaries. Air exposure causes a resistivity increase which may be attributed to experimental uncertainty but may also indicate a decrease in the surface scattering specularity upon Rh surface oxidation. The overall results suggest that Rh is a promising metal to potentially replace Cu for narrow interconnect lines. Particularly beneficial is the four times smaller λ of Rh in comparison to Cu, indicating a much reduced resistivity scaling. In addition, surface oxidation affects the Rh conductivity less than that of Cu. The small measured boundary reflection coefficient R = 0.16 also appears promising, but is for a high-symmetry grain boundary while the random boundary may have a considerably higher R. We note that a potential replacement of Cu by Rh will require extensive additional studies addressing the effect of the Rh-liner interface on the surface scattering, the Rh interconnect reliability, and processing performance cost tradeoffs.

- "Reliability study on cobalt and ruthenium as alternative metals for advanced interconnects," in 2017 IEEE International Reliability Physics Symposium (IRPS), 2017, pp. 6B-2.1-6B-2.8.
- [8] E. H. Sondheimer, "The mean free path of electrons in metals," Adv. Phys., vol. 1, no. 1, pp. 1–42, Jan. 1952, doi: 10.1080/00018735200101151.
- [9] K. Fuchs, "The conductivity of thin metallic films according to the electron theory of metals," *Math. Proc. Cambridge Philos. Soc.*, vol. 34, no. 1, pp. 100–108, Jan. 1938, doi: 10.1017/S0305004100019952.
- [10] D. K. C. Macdonald and K. Sarginson, "Size effect variation of the electrical conductivity of metals," *Proc. R. Soc. London. Ser. A. Math. Phys. Sci.*, vol. 203, no. 1073, pp. 223–240, Sep. 1950, doi: 10.1098/rspa.1950.0136.
- [11] A. F. Mayadas and M. Shatzkes, "Electrical-Resistivity Model for Polycrystalline Films: the Case of Arbitrary Reflection at External Surfaces," *Phys. Rev. B*, vol. 1, no. 4, pp. 1382–1389, Feb. 1970, doi: 10.1103/PhysRevB.1.1382.
- [12] J. S. Chawla, F. Gstrein, K. P. O'Brien, J. S. Clarke, and D. Gall, "Electron scattering at surfaces and grain boundaries in Cu thin films and wires," *Phys. Rev. B*, vol. 84, no. 23, p. 235423, Dec. 2011, doi: 10.1103/PhysRevB.84.235423.
- [13] C. Adelmann, K. Sankaran, S. Dutta, A. Gupta, S. Kundu, G. Jamieson, K. Moors, N. Pinna, I. Ciofi, S. van Elshocht, J. Bömmels, G. Boccardi, C. J. Wilson, G. Pourtois, and Z. Tökei, "Alternative Metals: From AB Initio Screening to Calibrated Narrow Line Models," in 2018 IEEE International Interconnect Technology Conference (IITC), Jun. 2018, pp. 154–156, doi: 10.1109/IITC.2018.8456484.
- [14] D. Gall, "Electron mean free path in elemental metals," J. Appl. Phys., vol. 119, no. 8, p. 085101, Feb. 2016, doi: 10.1063/1.4942216.
- [15] J. S. Chawla and D. Gall, "Specular electron scattering at single-crystal Cu(001) surfaces," *Appl. Phys. Lett.*, vol. 94, no. 25, p. 252101, Jun. 2009, doi: 10.1063/1.3157271.
- [16] P. Y. Zheng, R. P. Deng, and D. Gall, "Ni doping on Cu surfaces: Reduced copper resistivity," Appl. Phys. Lett., vol. 105, no. 13, p. 131603, Sep.

- 2014, doi: 10.1063/1.4897009.
- [17] V. Timoshevskii, Y. Ke, H. Guo, and D. Gall, "The influence of surface roughness on electrical conductance of thin Cu films: An ab initio study," J. Appl. Phys., vol. 103, no. 11, p. 113705, Jun. 2008, doi: 10.1063/1.2937188.
- [18] J. S. Chawla, F. Zahid, H. Guo, and D. Gall, "Effect of O2 adsorption on electron scattering at Cu(001) surfaces," *Appl. Phys. Lett.*, vol. 97, no. 13, p. 132106, Sep. 2010, doi: 10.1063/1.3489357.
- [19] F. Zahid, Y. Ke, D. Gall, and H. Guo, "Resistivity of thin Cu films coated with Ta, Ti, Ru, Al, and Pd barrier layers from first principles," *Phys. Rev. B*, vol. 81, no. 4, p. 045406, Jan. 2010, doi: 10.1103/PhysRevB.81.045406.
- [20] K. Barmak, A. Darbal, K. J. Ganesh, P. J. Ferreira, J. M. Rickman, T. Sun, B. Yao, A. P. Warren, and K. R. Coffey, "Surface and grain boundary scattering in nanometric Cu thin films: A quantitative analysis including twin boundaries," *J. Vac. Sci. Technol. A Vacuum, Surfaces, Film.*, vol. 32, no. 6, p. 061503, Nov. 2014, doi: 10.1116/1.4894453.
- [21] M. César, D. Liu, D. Gall, and H. Guo, "Calculated Resistances of Single Grain Boundaries in Copper," *Phys. Rev. Appl.*, vol. 2, no. 4, p. 044007, Oct. 2014, doi: 10.1103/PhysRevApplied.2.044007.
- [22] M. César, D. Gall, and H. Guo, "Reducing Grain-Boundary Resistivity of Copper Nanowires by Doping," *Phys. Rev. Appl.*, vol. 5, no. 5, p. 054018, May 2016, doi: 10.1103/PhysRevApplied.5.054018.
- [23] T.-H. Kim, X.-G. Zhang, D. M. Nicholson, B. M. Evans, N. S. Kulkarni, B. Radhakrishnan, E. A. Kenik, and A.-P. Li, "Large Discrete Resistance Jump at Grain Boundary in Copper Nanowire," *Nano Lett.*, vol. 10, no. 8, pp. 3096–3100, Aug. 2010, doi: 10.1021/nl101734h.
- [24] J. M. Rickman and K. Barmak, "Simulation of electrical conduction in thin polycrystalline metallic films: Impact of microstructure," *J. Appl. Phys.*, vol. 114, no. 13, p. 133703, Oct. 2013, doi: 10.1063/1.4823985.
- [25] L. Lu, Y. Shen, X. Chen, L. Qian, and K. Lu, "Ultrahigh Strength and High Electrical Conductivity in Copper," *Science*, vol. 304, no. 5669, pp. 422–426, Apr. 2004, doi: 10.1126/science.1092905.
- [26] T. Zhou, N. A. Lanzillo, P. Bhosale, D. Gall, and R. Quon, "A first-principles analysis of ballistic conductance, grain boundary scattering and vertical resistance in aluminum interconnects," AIP Adv., vol. 8, no. 5, p. 055127, May 2018, doi: 10.1063/1.5027084.
- [27] N. A. Lanzillo, "Ab Initio evaluation of electron transport properties of Pt, Rh, Ir, and Pd nanowires for advanced interconnect applications," *J. Appl. Phys.*, vol. 121, no. 17, p. 175104, May 2017, doi: 10.1063/1.4983072.
- [28] L. Brewer, "THE COHESIVE ENERGIES OF THE ELEMENTS," 1977. [Online]. Available: https://escholarship.org/uc/item/08p2578m.
- [29] S. Dutta, K. Sankaran, K. Moors, G. Pourtois, S. van Elshocht, J. Bömmels, W. Vandervorst, Zs. Tőkei, and C. Adelmann, "Thickness dependence of the resistivity of platinum-group metal thin films," *J. Appl. Phys.*, vol. 122, no. 2, p. 025107, Jul. 2017, doi: 10.1063/1.4992089.
- [30] K. Croes, C. Adelmann, C.J. Wilson, H. Zahedmanesh, O. V. Pedreira, C. Wu, A. Lesniewska, H. Oprins, S. Beyne, I. Ciofi, D. Kocaay, M. Stucchi, and Zs. Tőkei, "Interconnect metals beyond copper: Reliability challenges and opportunities," *Tech. Dig. Int. Electron Devices Meet. IEDM*, vol. 2018-Decem, pp. 5.3.1-5.3.4, 2019, doi: 10.1109/IEDM.2018.8614695.
- [31] D. Gall, "The search for the most conductive metal for narrow interconnect lines," J. Appl. Phys., vol. 127, no. 5, p. 050901, Feb. 2020, doi: 10.1063/1.5133671.
- [32] T. Zhou and D. Gall, "Resistivity scaling due to electron surface scattering in thin metal layers," *Phys. Rev. B*, vol. 97, no. 16, p. 165406, Apr. 2018, doi: 10.1103/PhysRevB.97.165406.
- [33] N. Trivedi and N. W. Ashcroft, "Quantum size effects in transport properties of metallic films," *Phys. Rev. B*, vol. 38, no. 17, pp. 12298– 12309, Dec. 1988, doi: 10.1103/PhysRevB.38.12298.
- [34] Z. Tešanović, M. V. Jarić, and S. Maekawa, "Quantum Transport and Surface Scattering," *Phys. Rev. Lett.*, vol. 57, no. 21, pp. 2760–2763, Nov. 1986, doi: 10.1103/PhysRevLett.57.2760.
- [35] G. Fishman and D. Calecki, "Influence of surface roughness on the conductivity of metallic and semiconducting quasi-two-dimensional structures," *Phys. Rev. B*, vol. 43, no. 14, pp. 11581–11585, May 1991, doi: 10.1103/PhysRevB.43.11581.
- [36] P. Y. Zheng, T. Zhou, B. J. Engler, J. S. Chawla, R. Hull, and D. Gall, "Surface roughness dependence of the electrical resistivity of W(001) layers," J. Appl. Phys., vol. 122, no. 9, p. 095304, Sep. 2017, doi: 10.1063/1.4994001.
- [37] Y.P. Timalsina, A. Horning, R. F. Spivey, K. M. Lewis, T.-S. Kuan, G.-C. Wang, and T.-M. Lu, "Effects of nanoscale surface roughness on the resistivity of ultrathin epitaxial copper films," *Nanotechnology*, vol. 26,

- no. 7, p. 075704, Feb. 2015, doi: 10.1088/0957-4484/26/7/075704.
- [38] D. Choi, X. Liu, P. K. Schelling, K. R. Coffey, and K. Barmak, "Failure of semiclassical models to describe resistivity of nanometric, polycrystalline tungsten films," *J. Appl. Phys.*, vol. 115, no. 10, p. 104308, Mar. 2014, doi: 10.1063/1.4868093.
- [39] E. Milosevic, S. Kerdsongpanya, M. E. McGahay, A. Zangiabadi, K. Barmak, and D. Gall, "Resistivity scaling and electron surface scattering in epitaxial Co(0001) layers," *J. Appl. Phys.*, vol. 125, no. 24, p. 245105, Jun. 2019, doi: 10.1063/1.5086458.
- [40] B. Wang and D. Gall, "Fully strained epitaxial Ti1-Mg N(001) layers," *Thin Solid Films*, no. January, p. 137165, Feb. 2019, doi: 10.1016/j.tsf.2019.02.028.
- [41] E. Milosevic, S. Kerdsongpanya, A. Zangiabadi, K. Barmak, K. R. Coffey, and D. Gall, "Resistivity size effect in epitaxial Ru(0001) layers," J. Appl. Phys., vol. 124, no. 16, p. 165105, Oct. 2018, doi: 10.1063/1.5046430.
- [42] S. S. Ezzat, P. D. Mani, A. Khaniya, W. Kaden, D. Gall, K. Barmak, and K. R. Coffey, "Resistivity and surface scattering of (0001) single crystal ruthenium thin films," *J. Vac. Sci. Technol. A*, vol. 37, no. 3, p. 031516, May 2019, doi: 10.1116/1.5093494.
- [43] K. Barmak, S. Ezzat, R. Gusley, A. Jog, S. Kerdsongpanya, A. Khanya, E. Milosevic, W. Richardson, K. Sentosun, A. Zangiabadi, D. Gall, W. E. Kaden, E. R. Mucciolo, P. K. Schelling, A. C. West, and K. R. Coffey, "Epitaxial metals for interconnects beyond Cu," J. Vac. Sci. Technol. A, vol. 38, no. 3, p. 033406, 2020, doi: 10.1116/6.0000018.
- [44] M. P. Delplancke, P. Delcambe, L. Binst, M. Jardinier-Offergeld, and F. Bouillon, "Structure and purity of epitaxial films of copper and rhodium deposited onto MgO single-crystal substrates by glow discharge sputtering," *Thin Solid Films*, vol. 143, no. 1, pp. 43–51, Sep. 1986, doi: 10.1016/0040-6090(86)90145-8.
- [45] T. Zhou, P. Zheng, S. C. Pandey, R. Sundararaman, and D. Gall, "The electrical resistivity of rough thin films: A model based on electron reflection at discrete step edges," *J. Appl. Phys.*, vol. 123, no. 15, p. 155107, Apr. 2018, doi: 10.1063/1.5020577.
- [46] G. K. White and S. B. Woods, "Electrical and Thermal Resistivity of the Transition Elements at Low Temperatures," *Philos. Trans. R. Soc. A Math. Phys. Eng. Sci.*, vol. 251, no. 995, pp. 273–302, Mar. 1959, doi: 10.1098/rsta.1959.0004.
- [47] E. Milosevic, P. Zheng, and D. Gall, "Electron Scattering at Epitaxial Ni(001) Surfaces," *IEEE Trans. Electron Devices*, vol. 66, no. 10, pp. 4326–4330, Oct. 2019, doi: 10.1109/TED.2019.2934636.
- [48] E. Milosevic, S. Kerdsongpanya, M. E. McGahay, B. Wang, and D. Gall, "The Resistivity Size Effect in Epitaxial Nb(001) and Nb(011) Layers," *IEEE Trans. Electron Devices*, vol. 66, no. 8, pp. 3473–3478, Aug. 2019, doi: 10.1109/TED.2019.2924312.
- [49] R. Powell, R. Tye, and M. Woodman, "Thermal conductivities and electrical resistivities of the platinum metals," *Platin. Met. Rev*, vol. 6, pp. 138–143, 1962, [Online]. Available: http://www.platinummetalsreview.com/pdf/pmr-v6-i4-138-143.pdf.
- [50] P. Zheng and D. Gall, "The anisotropic size effect of the electrical resistivity of metal thin films: Tungsten," *J. Appl. Phys.*, vol. 122, no. 13, p. 135301, Oct. 2017, doi: 10.1063/1.5004118.
- [51] J. J. Plombon, E. Andideh, V. M. Dubin, and J. Maiz, "Influence of phonon, geometry, impurity, and grain size on Copper line resistivity," *Appl. Phys. Lett.*, vol. 89, no. 11, p. 113124, Sep. 2006, doi: 10.1063/1.2355435.
- [52] J.-W. Lim, K. Mimura, and M. Isshiki, "Thickness dependence of resistivity for Cu films deposited by ion beam deposition," *Appl. Surf. Sci.*, vol. 217, no. 1–4, pp. 95–99, Jul. 2003, doi: 10.1016/S0169-4332(03)00522-1.